

Arginine Methylation Regulates MEIS2 Nuclear Localization to Promote Neuronal Differentiation of Adult SVZ Progenitors

Jasmine Kolb,^{1,4} Marie Anders-Maurer,¹ Tanja Müller,¹ Ann-Christin Hau,^{1,5} Britta Moyo Grebbin,^{1,6} Wiebke Kallenborn-Gerhardt,² Christian Behrends,^{3,7} and Dorothea Schulte^{1,*}

¹Institute of Neurology, Edinger Institute, University Hospital Frankfurt, 60528 Frankfurt, Germany

²Institute of Pharmacology, College of Pharmacy, Goethe University, 60438 Frankfurt, Germany

³Institute of Biochemistry II, University Hospital Frankfurt, 60528 Frankfurt, Germany

⁴Present address: Dr. Ehrlich Pharma, 88410 Bad Wurzach, Germany

⁵Present address: Luxembourg Institute of Health, 84 Val Fleuri, 1526 Luxembourg, Luxembourg

⁶Present address: Institute for Tumorbiology and Experimental Therapy, Georg-Speyer-Haus, 60596 Frankfurt, Germany

⁷Present address: Ludwig-Maximilians-Universität München, Munich Cluster of Systems Neurology, 81377 Munich, Germany

*Correspondence: dorothea.schulte@kgu.de

<https://doi.org/10.1016/j.stemcr.2018.03.010>

SUMMARY

Adult neurogenesis is regulated by stem cell niche-derived extrinsic factors and cell-intrinsic regulators, yet the mechanisms by which niche signals impinge on the activity of intrinsic neurogenic transcription factors remain poorly defined. Here, we report that MEIS2, an essential regulator of adult SVZ neurogenesis, is subject to posttranslational regulation in the SVZ olfactory bulb neurogenic system. Nuclear accumulation of MEIS2 in adult SVZ-derived progenitor cells follows downregulation of EGFR signaling and is modulated by methylation of MEIS2 on a conserved arginine, which lies in close proximity to nested binding sites for the nuclear export receptor CRM1 and the MEIS dimerization partner PBX1. Methylation impairs interaction with CRM1 without affecting PBX1 dimerization and thereby allows MEIS2 nuclear accumulation, a prerequisite for neuronal differentiation. Our results describe a form of posttranscriptional modulation of adult SVZ neurogenesis whereby an extrinsic signal fine-tunes neurogenesis through posttranslational modification of a transcriptional regulator of cell fate.

INTRODUCTION

Postnatal neurogenesis contributes to homeostasis and plasticity in the adult brain by the addition of new neurons and the replacement of old ones in existing network circuitries. In the mammalian forebrain, adult generation of neurons is restricted to few privileged areas, including the subventricular zone (SVZ) and the dentate gyrus (DG) of the hippocampus. The SVZ harbors astroglial-like stem cells, which generate transient amplifying progenitor cells (TAPs) that, after few cell divisions, mature into neuroblasts. Whereas TAPs can still generate both neurons and glia, neuroblasts are committed to the neuronal lineage and already possess traits of immature neurons, such as staining positive for the microtubule-associated protein doublecortin (DCX), the neuron-specific class III β -tubulin (recognized by the TuJ1 antibody), or the polysialylated form of neural cell adhesion molecule (PSA-NCAM). In rodents, SVZ-generated neuroblasts migrate into the olfactory bulb (OB) where they differentiate mostly into inhibitory olfactory interneurons (Hsieh, 2012; Ming and Song, 2011). Continuous SVZ neurogenesis is crucial for the structural and functional integrity of the adult OB and for olfaction-associated behavior (Imayoshi et al., 2008; Sakamoto et al., 2011). In contrast to the developing brain, where the generation of neuronal cell types follows a stereotypic spatial and temporal order, adult neurogenesis

is strongly influenced by environmental signals. Examples include the increased generation of granule cells in the DG after physical activity or the modulation of adult SVZ neurogenesis by hormonal changes or in response to hypothalamic innervation (Kempermann et al., 1997; Paul et al., 2017; Shingo et al., 2003). Adult neural stem and progenitor cells thus activate intrinsic neurogenic programs in response to extrinsic signals, which reflect the physiological state of the organism. The molecular pathways by which niche-derived signals are relayed onto transcriptional regulators of cellular differentiation, however, are still poorly defined.

MEIS (myeloid ectopic viral integration site) family proteins belong to the atypical TALE class of homeodomain-containing transcription factors. They function as part of heteromeric complexes with the related PBX (pre-B cell leukemia homeobox) proteins and act synergistically with other transcriptional regulators, including HOX and PAX proteins (Ladam and Sagerström, 2014; Longobardi et al., 2014; Schulte, 2014). In the SVZ, neuronal differentiation requires MEIS2, as *Meis* knockdown or transduction of a function-blocking protein enhanced gliogenic differentiation at the expense of neurogenic differentiation *in vitro* and *in vivo* (Agoston et al., 2014). Mechanistically, MEIS2 recruits the histone modifier PARP1/ARTD1 to transcriptionally inactive, but PBX1-prebound sites in the regulatory regions of neuron-specific genes, thereby facilitating



poly-ADP ribosylation of the linker histone H1 at these sites, which is followed by local decompaction of the chromatin fiber and effective gene expression (Hau et al., 2017). MEIS2-mediated recruitment of PARP1 to chromatin hence constitutes an important early step in the *de novo* activation of neuron-specific genes. Surprisingly, *Meis2* transcripts are already present in quiescent adult neural stem cells in the SVZ, whereas robust MEIS2 immunoreactivity is first seen in neuroblasts (Agoston et al., 2014; Beckervordersandforth et al., 2010). MEIS2 must therefore be under particularly stringent posttranscriptional or posttranslational control in the SVZ, yet the underlying mechanisms are still largely unknown.

RESULTS AND DISCUSSION

MEIS2 Subcellular Localization in SVZ-Derived Progenitor Cells Is Regulated by EGFR Signaling

Adult SVZ-derived stem cells and TAPs grown as primary, free-floating neurospheres (aNS) in the presence of epidermal growth factor (EGF) and basic fibroblast growth factor (FGF2) already possess high levels of *Meis2* transcripts, which increase further during neuronal differentiation, but only faint MEIS2 immunoreactivity (Figures 1A, 1B, and S1). Notably, MEIS2 protein in these cells is evenly distributed between cytoplasm and nucleus, as observed with antibodies directed against different epitopes of the MEIS2 protein (Figures 1B and 1C). In the SVZ *in vivo*, most TAPs (identified as bromodeoxyuridine-positive (BrdU+) cells following a short BrdU pulse or by the Ki67 antigen) also exhibited weak nucleo-cytoplasmic MEIS2 staining (Figures 1D and S1). By contrast, adult SVZ stem cells isolated by their co-expression of GFAP and prominin or putative stem cells *in vitro* (defined as label-retaining, nestin-positive aNS cells, pulse labeled with carboxyfluorescein diacetate succinimidyl ester) are MEIS2 immunonegative (Beckervordersandforth et al., 2010; Figure S1). When SVZ-derived aNS cells were induced to differentiate by removal of EGF and FGF2 from the culture medium and plating on laminin, MEIS2 protein rapidly localized to the nucleus of some cells in the cultures, and these cells began to stain positive for the early neuronal marker PSA-NCAM (Figure 1C). Accumulation of MEIS2 in the cell nucleus is thus a very early sign of neuronal differentiation.

Activated stem cells and proliferating TAPs express EGF receptor (EGFR), and EGFR activation promotes proliferation and counteracts neuronal differentiation *in vivo* and *in vitro* (Doetsch et al., 2002). We therefore induced cellular differentiation in aNS by adding the EGFR inhibitor Tyrophostin AG1478 to EGF/FGF2-containing culture medium and assessed MEIS2 nucleo-cytoplasmic redistribution 8 hr later (Figures 1F–1H and S1). Cells in which nuclear MEIS2

immunoreactivity predominated over that in the cytoplasm were defined as “nuclear accumulation” (e.g., arrowheads in Figures 1C₂–1C₄, middle panels), and cells with uniform MEIS2 staining in cytoplasm and nucleus upon differentiation were counted as “cytoplasmic retention” (e.g., arrows in Figures 1C₂ and 1C₃). Treatment with AG1478 elevated the proportion of cells in which MEIS2 accumulated in the cell nucleus 10-fold, while treatment with the FGFR1 inhibitor SU5402 did not (Figures 1F–1H). We concluded that MEIS2 subcellular localization is regulated in response to EGFR signaling.

Neuronal Differentiation Requires Nuclear Accumulation of MEIS2

In silico analysis of the MEIS2 polypeptide sequence identified a nuclear localization signal (NLS) (amino acids 274–280 of NCBI CAA04139.1) and a canonical nuclear export signal (NES) (amino acids 161–163), suggesting that MEIS2 continuously shuttles between nucleus and cytoplasm (Figure 2A). The nuclear accumulation of MEIS2 that accompanies neuronal differentiation must hence involve activation of the NLS and/or silencing of the NES. Remarkably, the NES is fully embedded in a previously identified binding surface for the MEIS dimerization partner PBX (Figure 2A, Knoepfler et al., 1997). We therefore hypothesized that PBX and the nuclear export receptor CRM1 may compete for binding to MEIS2, and that this competition may regulate MEIS2 subcellular localization. We blocked CRM1-dependent nuclear export with leptomycin B (LMB) in aNS grown in EGF/FGF2-containing medium. Eight hours of LMB treatment significantly induced nuclear accumulation of MEIS2 (Figures 2B–2D; 8 hr LMB: 3.33% ± 0.87%, ctrl: 1.22% ± 0.81%). Strikingly, LMB treatment also induced the generation of neurons in these cultures, evident in a more than 3-fold increase in cells labeling for TuJ1 (8 hr LMB: 2.75% ± 0.91%, ctrl: 0.85% ± 0.28%; Figures 2E–2G). Neurogenesis thus occurred despite the fact that the cells were grown in the presence of EGF and FGF2, and hence under conditions that normally preclude cellular differentiation. Adult SVZ-derived progenitor cells thus exist in a delicate “meta-stable” state, which is maintained by the continuous CRM1-dependent export of differentiation-inducing protein(s) from the nucleus. To investigate whether MEIS2 is such a protein, we transduced *Meis2*, C-terminally fused to a triple HA tag and either the strong NLS from SV40 large T antigen or the NES from the HIV tat protein into aNS, induced cellular differentiation 48 hr later, and scored the fate of the transduced cells after 3 days (Figure 2H). Forced nuclear import of MEIS2 increased, whereas forced nuclear export decreased neuron production in these cultures relative to wild-type (WT) MEIS2 (TuJ1+ cells: WT *Meis2* 13.30% ± 3.26%, *Meis2*-NES 5.17% ± 2.71%, *Meis2*-NLS 22.85% ± 2.87%; Figure 2I).

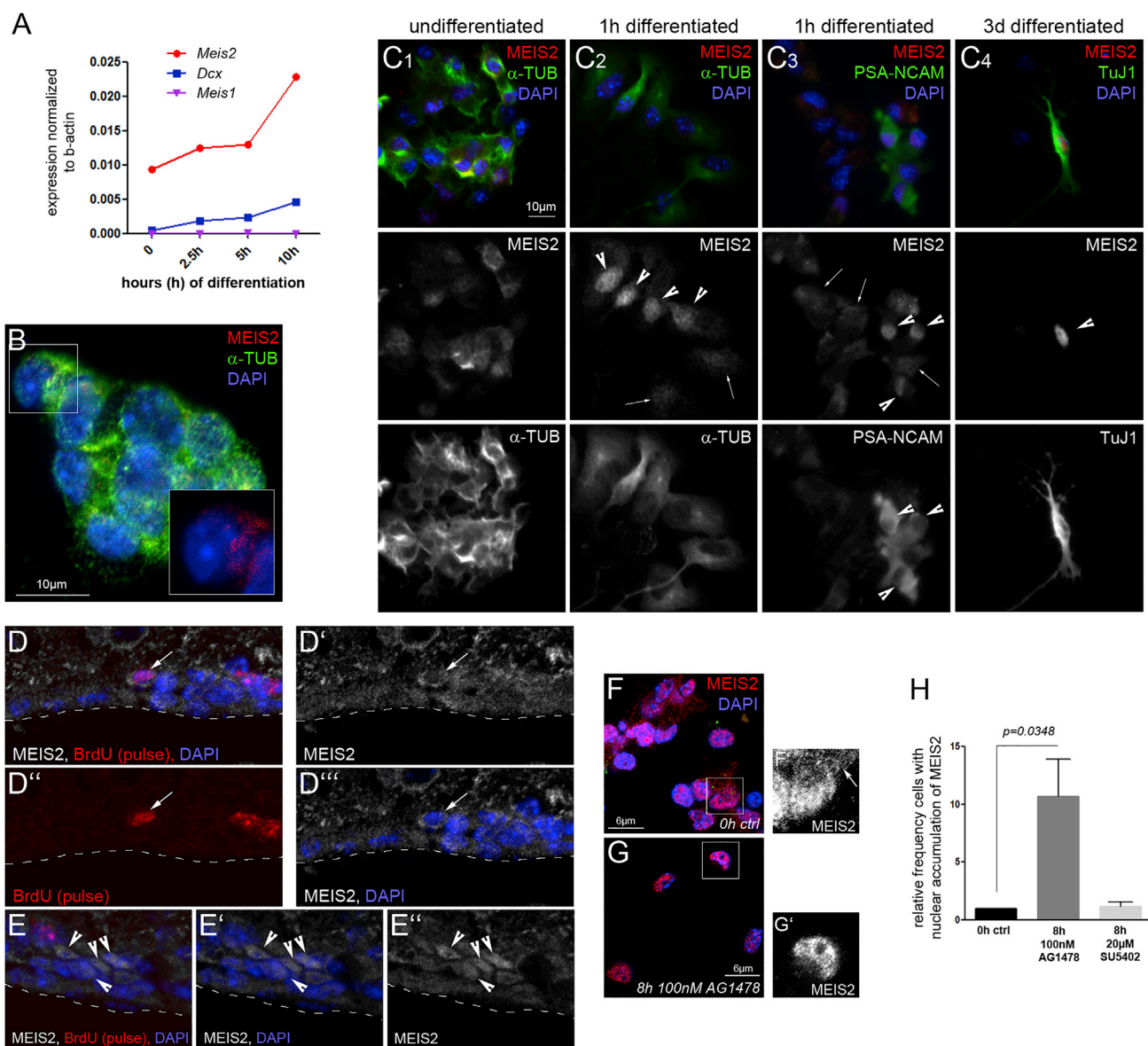


Figure 1. MEIS2 Protein Stability and Subcellular Localization in SVZ-Derived Progenitor Cells Is Controlled by EGFR Signaling
 (A) Transcript levels (determined by qPCR) of *Meis1*, *Meis2*, and *Dcx* in primary aNS after induction of neuronal differentiation for the times indicated.
 (B) Primary, free-floating aNS stained for MEIS2 (red) and α -tubulin (green); MEIS2 immunoreactivity in cells of the boxed area is shown as insert.
 (C) Expression of MEIS2 relative to α -tubulin or the neuron-specific markers PSA-NCAM and TuJ1 in undifferentiated primary aNS, after 1 hr or 3 days of differentiation; arrowheads indicate nuclear accumulation of MEIS2 (middle panel) or PSA-NCAM staining (lower panel); arrows indicate uniform cellular MEIS2 distribution typical of progenitor cells. Scale bars, 10 μ m (applies to all panels).
 (D and E) Weak, uniform MEIS2 staining in BrdU pulse-labeled TAPs in the SVZ *in vivo*; the arrows in (D) indicate a BrdU-positive cell with MEIS2 cytoplasmic staining; the arrowheads in (E) indicate BrdU-negative, MEIS2-positive putative chain-migrating neuroblasts; BrdU, red; MEIS2, white.
 (F and G) Eight hours of treatment with AG1478 (F), but not DMSO as control (G), induces nuclear accumulation of MEIS2 in primary aNS growing in the presence of EGF/FGF2.
 (H) Quantification of the results for AG1478, SU5402, and DMSO; n = 3 independent experiments. Data are represented as means \pm SEM. See also Figure S1.

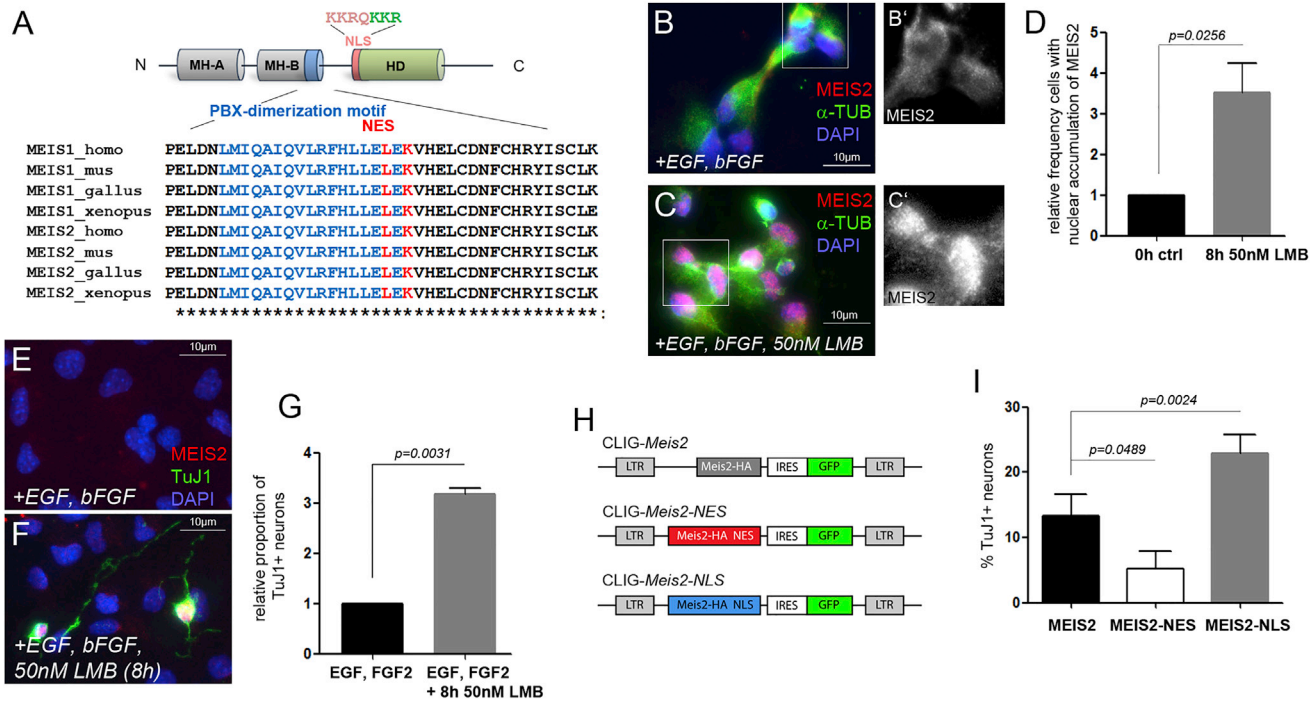


Figure 2. Neuronal Differentiation Requires Nuclear Accumulation of MEIS2

(A) Sequence and relative location of the PBX-interacting motif, NES, and NLS found in Meis family members in different vertebrate species.
 (B and C) Subcellular localization of MEIS2 in primary aNS without LMB (B) or treated with LMB (C); MEIS2 immunofluorescence of the boxed areas is shown as single channel in (B' and C').
 (D) Quantification of the results; $n = 5$ independent experiments.
 (E and F) Inhibition of nuclear export by LMB (F) induces neuronal differentiation in aNS growing in EGF/FGF2-containing medium.
 (G) Quantification of the results; $n = 3$ independent experiments.
 (H) Schematic representation of the retroviral vectors used in (I).
 (I) Retroviral transduction of *Meis2-NLS* enhances, whereas transduction of *Meis2-NES* reduces neurogenesis relative to WT-*Meis2* ($n = 4$ independent experiments).
 Data in (D), (G), and (I) are represented as means \pm SEM. See also [Figure S2](#).

Availability of MEIS2 in the cell nucleus is therefore a rate-limiting determinant of neuronal differentiation of adult SVZ-derived neural progenitor cells.

Although MEIS proteins usually function as components of larger protein complexes, requirement for an otherwise essential binding partner can be overcome by fusion of MEIS to a dominant transactivation domain (Mamo et al., 2006; Wang et al., 2006). Because MEIS2 and PAX6 co-operate in SVZ neurogenesis, we reasoned that *Meis2* fused to the VP16 transactivation domain together with an NLS (*Meis2-VP16-NLS*) may mimic the combined activities of nuclear MEIS2 and PAX6. Indeed, retroviral transduction of *Meis2-VP16-NLS* into free-floating aNS induced massive generation of neurons even in EGF/FGF2-containing medium (Figure S2). When localized to the cell nucleus and in conjunction with a strong transactivation domain, MEIS2 is thus able to direct neurosphere-derived cells

toward neurogenesis under conditions that normally preclude neuronal differentiation.

PBX1 and CRM1 Compete for Binding to MEIS2

We directly compared recombinant PBX1 and CRM1 for binding with a synthetic peptide comprising the PBX1-binding motif and NES of MEIS2 (amino acids 146–180 of NCBI CAA04139.1) (Figure 3A). Immobilized peptides were incubated with PBX1 or CRM1, produced by *in vitro* transcription/translation. Both CRM1 and PBX1 were enriched by the peptide with CRM1 binding affinity exceeding that of PBX1 (Figure 3A). Pre-incubation of the peptide with *in vitro*-translated PBX1 blocked CRM1 binding to MEIS2^{146–180}, even when excessive amounts of CRM1 were added to the reaction (Figure 3B). CRM1 thus fails to recognize the NES in a PBX1-MEIS2 heterodimer.

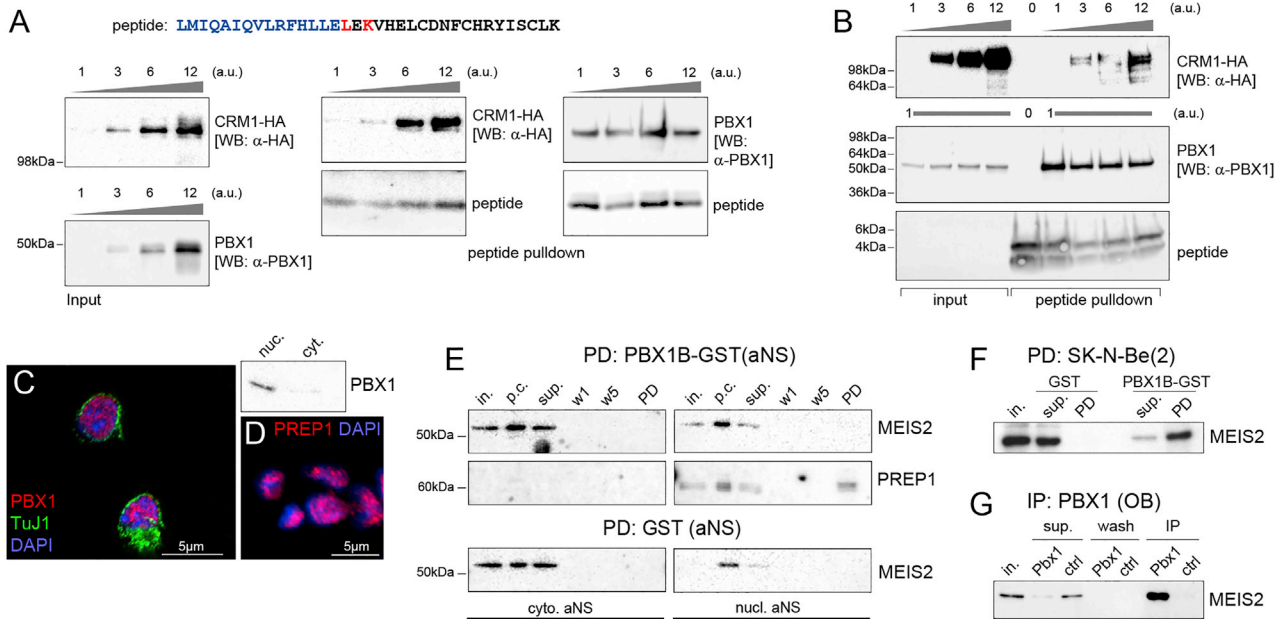


Figure 3. PBX1 and CRM1 Compete for Association with MEIS2

(A) *In vitro* pull-down (PD) assays with synthetic MEIS2 peptides; (left) input: *in vitro*-translated CRM1-HA or PBX1; band intensities correspond to 30% of the protein used for the PD; (middle) PD with CRM1; (right) PD with PBX1. Lower bands: biotinylated peptide eluted from the streptavidin-coated beads. Peptide sequence: PBX dimerization motif, blue; NES, red.

(B) Competitive *in vitro* pull-down assay with MEIS2^{146–180} peptides that were pre-incubated with constant amounts of *in vitro*-translated PBX1 followed by addition of increasing amounts of *in vitro*-translated CRM1-HA.

(C and D) PBX1 (C) and PREP1 (D) are nuclear in primary aNS.

(E) PBX1-GST precipitates PREP1, but not MEIS2, from aNS extracts.

(F) MEIS2 co-precipitates with PBX1-GST from nuclear extracts of SK-N-Be(2) cells.

(G) Co-immunoprecipitation of PBX1 and MEIS2 from the OB. in, input; p.c., preclear; sup., supernatant; w, wash; PD, precipitate of the pull-down; IP, immunoprecipitate; ctrl., isotype-specific control.

Binding of PBX1 to either MEIS or PREP induces nuclear localization of the heterodimer in different physiological contexts (Berthelsen et al., 1998; Mercader et al., 1999). We therefore focused on MEIS-PBX dimer formation. In primary adult SVZ-derived aNS, *PBX1*, *PREP1*, and *MEIS2* are co-expressed, yet only PBX1 and PREP1 localize to the cell nucleus, suggesting that PBX1 may exclusively dimerize with PREP1 in these cells (Figures 3C and 3D). Indeed, pull-down experiments with GST-tagged PBX1 and protein extracts prepared from the nuclear or cytoplasmic compartment of primary aNS enriched PREP1, but not MEIS2 (Figure 3E). Yet, MEIS2 was readily precipitated by PBX1-GST from extracts of SK-N-Be(2) cells or in complex with PBX1 by immunoprecipitation from extracts of adult OB neurons, two cell populations in which MEIS2 localizes to the cell nucleus (Figures 3F and 3G).

Differential Methylation of Arginine 174 Modulates MEIS2 Association with CRM1 or PBX1

We purified MEIS2 from primary SVZ-derived aNS and primary OB tissue and examined both protein fractions by

mass spectrometry (MS) (Figures 4A and 4B). Interestingly, MEIS2 purified from the OB but not from aNS carried a mono-methylation on a conserved arginine at position 174 (R¹⁷⁴; Figures 4A and 4B). R¹⁷⁴ lies in close proximity to the overlapping NES- and PBX1-binding motifs, raising the possibility that methylation at this position may regulate MEIS2 nucleo-cytoplasmic localization by altering its affinity toward PBX1 or CRM1 (Figure S3). To test this hypothesis, we first induced primary aNS to differentiate for 4 hr in the presence or absence of adenosine-2',3'-dialdehyde (AdOX), a general inhibitor of protein arginine methyltransferases (PRMTs). Whereas MEIS2 largely accumulated in the nucleus in control-treated cultures, strong cytoplasmic MEIS2 staining was seen in AdOX-treated cells (Figures 4C–4E). Inhibition of arginine methylation thus prevented the nuclear accumulation of MEIS2 that normally accompanies neuronal differentiation. To investigate whether methylation on R¹⁷⁴ was involved, we misexpressed HA-tagged MEIS2 or a mutant form of MEIS2 in which R¹⁷⁴ was replaced with alanine (MEIS2^{R174A}) in aNS. Nuclear accumulation of MEIS2^{R174A} was severely

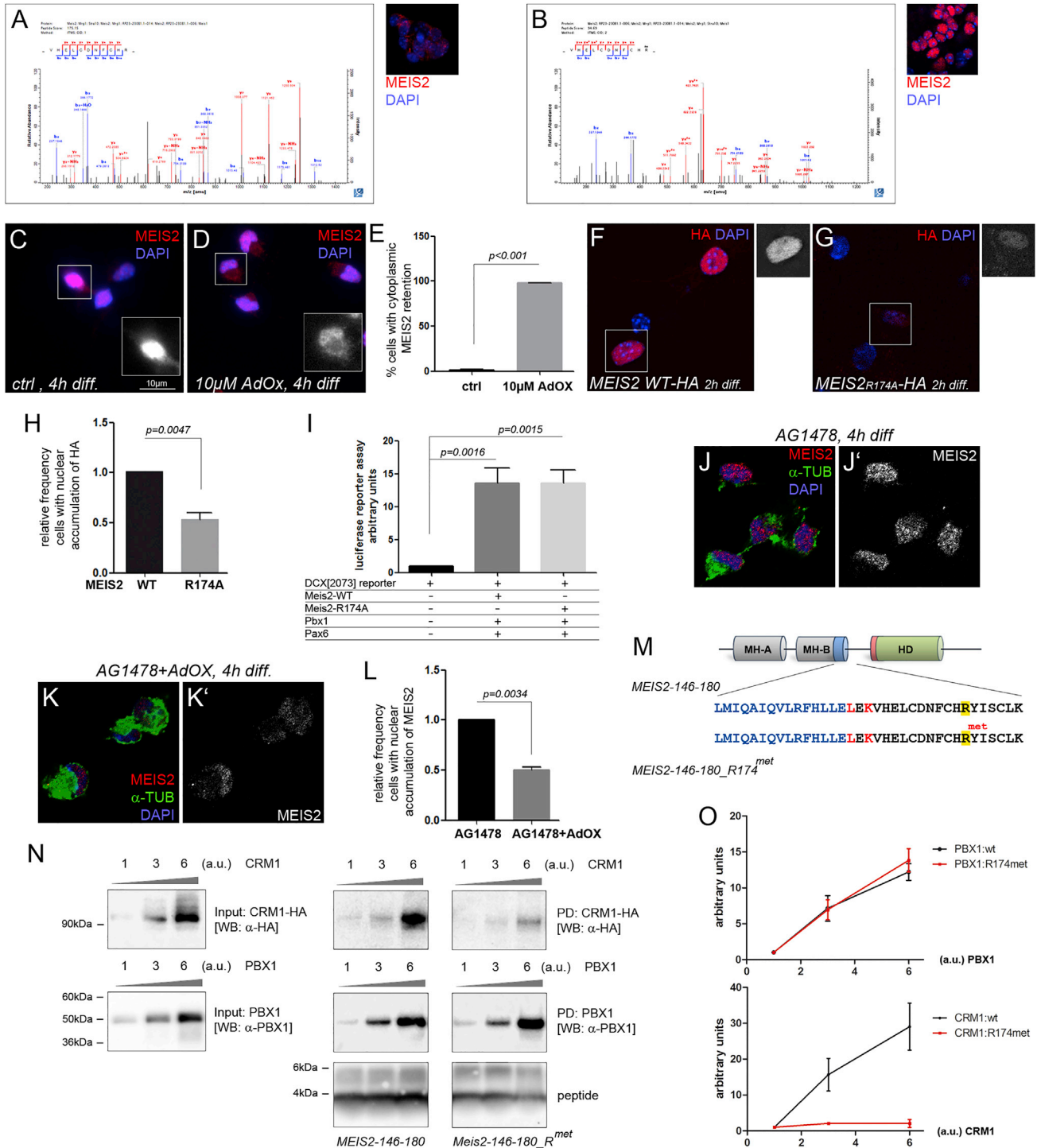


Figure 4. Methylation on R¹⁷⁴ Modulates CRM1 Binding and Nuclear Localization of MEIS2

(A and B) MS/MS spectra of peptides derived from MEIS2 isolated from aNS (A) and OB (B), methyl modifications at R174 indicated by “me” (B); the insets show non-nuclear and nuclear MEIS2 immunoreactivity in SVZ-derived aNS and OB, respectively.

(C and D) Inhibition of protein methylation by AdOX (D) prevents nuclear accumulation of MEIS2 upon differentiation; (C) control. MEIS2 immunoreactivity in the boxed cells is shown as inserts.

(E) Quantification of the results; n = 3 independent experiments.

(legend continued on next page)



compromised following 2 hr of differentiation compared with WT-MEIS2 (Figures 4F–4H). A reporter construct in which luciferase is expressed under control of the proximal enhancer/promoter of the *DCX* gene is activated by MEIS2 together with PBX1 and PAX6 when used in a reporter assay in HEK293T cells (Agoston et al., 2014). MEIS2^{R174A} was fully functional in this assay, demonstrating that post-translational modification on R¹⁷⁴ influences the subcellular localization of the protein but not its ability to activate transcription (Figure 4I). Because EGFR inhibition by AG1478 had been sufficient to induce nuclear localization of MEIS2 in free-floating aNS (Figure 1), we treated aNS with AG1478 together with AdOX, reasoning that AG1478-induced nuclear accumulation of MEIS2 might be precluded by AdOX if R¹⁷⁴ methylation was occurring as a result of EGFR pathway inhibition. Indeed, significantly fewer cells exhibited nuclear accumulation of MEIS2 after 4 hr of combined treatment with AG1478 and AdOX than after treatment with AG1478 alone (AG1478: 5.52% ± 1.8%; AG1478 + AdOX: 2.7% ± 0.9%; Figures 4J–4L). Collectively, these observations argue that the nucleo-cytoplasmic redistribution of MEIS2 upon EGFR pathway inhibition acts via differential methylation of MEIS2 on R¹⁷⁴. We therefore directly compared recombinant PBX1 and CRM1 for binding with synthetic peptides that were either non-methylated (MEIS2^{146–180}) or methylated on R¹⁷⁴ (MEIS2^{146–180met}; Figure 4M). Whereas PBX1 alone co-precipitated equally well with the methylated and non-methylated peptide, CRM1 bound more strongly to MEIS2^{146–180} than to MEIS2^{146–180met} (Figures 4N and 4O). Methylation at R¹⁷⁴ thus reduces MEIS2 affinity for CRM1 and thereby indirectly favors its association with PBX1.

In sum, nuclear localization of a MEIS family protein and its ability to dimerize with PBX can be jointly regulated by methylation on an evolutionary conserved arginine resi-

due. Although it is well established that nuclear localization of PBX1 or its *D. melanogaster* homolog *extradenticle* (*exd*) requires association with an MEIS family dimerization partner (Abu-Shaar et al., 1999; Berthelsen et al., 1999), the results presented here establish an additional level of complexity by demonstrating that the subcellular localization of MEIS itself is modulated by posttranslational modification as a function of cellular differentiation. In addition, our results provide evidence for a mode by which adult SVZ neurogenesis can be quickly fine-tuned in response to extracellular signals: in adult SVZ progenitor cells, non-methylated MEIS2 is rendered inactive by continuous CRM1-dependent nuclear export. Methylation on R¹⁷⁴ weakens CRM1 binding to MEIS2 and thereby facilitates MEIS2 dimerization with PBX1 and its accumulation in the cell nucleus, an established prerequisite for neuronal differentiation (Agoston et al., 2014; Hau et al., 2017). On the molecular level, methylation on R¹⁷⁴ may modulate MEIS2 subcellular distribution either directly by steric interference with CRM1 binding or more indirectly by inducing a conformational change in the MEIS2 polypeptide chain, which then masks the NES. Our observation that methylation on R¹⁷⁴ decreased binding of CRM1 to the MEIS2 NES in a peptide of only 35 amino acids in length argues that R¹⁷⁴ methylation directly impacts on CRM1 binding. Notably, *in silico* protein structure predictions indicate that the MH-B domain of MEIS2, harboring the PBX-binding motif, NES, and R174, forms an α -helical secondary structure in solution, which condenses the 11 amino acid distance between R¹⁷⁴ and the NES to three helical turns, bringing R¹⁷⁴ and the NES in even closer proximity (Figure S3).

Because inhibition of PRMTs by AdOX counteracted the nuclear accumulation of MEIS2, which is normally induced by AG1478 treatment, EGFR pathway inhibition likely plays a major role in R¹⁷⁴ methylation of MEIS2.

(F and G) Subcellular localization of HA-tagged WT-MEIS2 (F) and MEIS2-R174A (G) in aNS after 2 hr of differentiation; MEIS2 immunoreactivity in the boxed cells is shown in separate panels.

(H) Quantification of the results; n = 4 independent experiments.

(I) Luciferase reporter assay in HEK293T cells: a 2073 basepair fragment of the murine *DCX* promoter/proximal enhancer is transcriptionally activated by PBX1 and PAX6 together with WT-MEIS2 or MEIS2^{R174A}; n = 7 independent experiments.

(J and K) Subcellular distribution of MEIS2 after 4 hr of treatment with AG1478 alone (J) or in combination with AdOX (K); MEIS2 immunofluorescence is shown as separate panels in (J' and K').

(L) Quantification of the results; n = 3 independent experiments.

(M) Amino acid sequence of the methylated and non-methylated MEIS2 peptides.

(N) Different binding affinities of PBX1 and CRM1 to methylated and non-methylated peptides; (left) input: *in vitro*-translated CRM1-HA or PBX1; (middle) PD with non-methylated MEIS2^{146–180}; (right) PD with MEIS2^{146–180} methylated on R¹⁷⁴. The lower panels show the biotinylated peptide eluted from the streptavidin-coated beads.

(O) Densitometric quantification of the band intensities of PBX1 (left) and CRM1 (right) bound to non-methylated (WT, black) or methylated peptide (R174met, red) as shown in (N); n = 4 independent experiments. PD, precipitate of the pull-down. The lowest band intensity was set as a.u. 1. PBX1 binds with equal affinities to both peptides, whereas CRM1 prefers the non-methylated form.

Data in (E), (H), (I), (L), and (O) are represented as means ± SEM.



Downregulation of EGFR signaling *in vitro* is achieved by removing EGF from the culture medium, an integral step in virtually all *in vitro* differentiation protocols for adult neural stem and progenitor cells. In the SVZ *in vivo*, the process is undoubtedly more complex and likely involves the integration of multiple extracellular signals, possibly together with the spatial displacement of progenitor cells from the influence of the stem cell niche. Irrespective of how EGFR signaling is terminated, the data presented here highlight how extracellular signals can impinge on a transcriptional regulator of neurogenic differentiation.

EXPERIMENTAL PROCEDURES

Experiments Involving Animals and Cell Culture

Sphere-forming cells were isolated from 7- to 10-week-old C57BL/6 mice, cultured, and retrovirally transduced following published protocols (Agoston et al., 2014). All procedures involving animals were approved by the local animal care committee and the government of Hessen and are in accordance with German and EU regulations. SK-N-BE(2) and HEK293T cells were cultured following standard conditions. For pharmacological inhibitors, plasmids, and small interfering RNAs, see Supplemental Information.

Retroviral Constructs

Full-length *Meis2b* was C-terminally fused to a triple HA tag and cloned into the retroviral vector pCLIG (Agoston et al., 2014). *Meis2-NLS* and *Meis2-NES* carry oligonucleotides corresponding to the NLS of SV40 large T antigen (PKKKRKV) or the NES of the HIV-1 tat protein, respectively, inserted in frame in the HA tag of *mMeis2b-HA*. In CLIG-*Meis2-NLS-VP16*, mMEIS2b-HA was C-terminally fused to the SV40 large T antigen NLS followed by an in-frame fusion to the herpes simplex virion protein 16 transactivation domain. In CLIG-*Meis2-R174A*, the arginine at position 174 of mMEIS2b-HA was converted into alanine by site-directed mutagenesis (Phusion Site-Directed Mutagenesis Kit, Thermo Scientific, F-541). Luciferase reporter assays were performed as described in Agoston et al. (2014).

MS Analysis

Peptide mixtures derived from in-gel tryptic digests of SDS-PAGE-separated MEIS2 immunoprecipitates were analyzed by liquid chromatography-tandem MS (LC-MS/MS) using an EasyLC nano-HPLC coupled to an Orbitrap Elite mass spectrometer (both Thermo Scientific). MS raw data were processed by MaxQuant (Cox and Mann, 2008) with methylation of arginine and lysine set as variable modifications.

Peptide Pull-Down

Peptides comprising the sequences LMIQAIQVLRFHLELEKVVH ELCDNFCHRYISCLK and LMIQAIQVLRFHLELEKVVHLELDCNF CHR{met}YISCLK, N-terminally linked to a mini-PEG linker followed by biotin (ProteoGenix; Schiltigheim, France), were immobilized on streptavidin-coated Dynabeads (Invitrogen) in 20 mM sodium phosphate (pH 7.4), 150 mM KCl, 0.5 mM EDTA,

5 mM MgCl₂, 10% glycerol, cOmplete protease inhibitor cocktail (Roche), washed, blocked with 0.1% BSA, and incubated with different amounts of recombinant PBX1 or CRM1-HA generated by TNT-coupled transcription/translation (Promega) for 2 hr at 4°C. For competitive pull-down assays, peptide-loaded beads were pre-incubated with PBX1 for 30 min prior to the addition of CRM1-HA. Proteins were resolved by SDS-PAGE and detected by western blot with antibodies against PBX1 (Chemicon), hemagglutinin (HA) (Roche) to detect CRM1-HA or horseradish peroxidase-coupled streptavidin to detect the biotinylated peptide. For the quantification shown in Figure 4O, band intensity was determined densitometrically with ImageJ.

SUPPLEMENTAL INFORMATION

Supplemental Information includes Supplemental Experimental Procedures and three figures and can be found with this article online at <https://doi.org/10.1016/j.stemcr.2018.03.010>.

AUTHOR CONTRIBUTIONS

J.K., M.A.M., T.M., A.C.H., B.M.G., and W.K.G. performed the experiments. C.B. performed MS analysis. D.S. and J.K. designed the study. D.S. wrote the manuscript.

ACKNOWLEDGMENTS

We thank Ralph Kehlenbach (University Medical School Göttingen) and Licia Selleri (University of California, San Francisco) for reagents. The work was supported by the Deutsche Forschungsgemeinschaft (SCHU1218/3-3 to D.S. and BE4685/1-1 to C.B.), the August Scheidel-Foundation, the Schram-Foundation, and the Ludwig Edinger-Foundation.

Received: October 16, 2017

Revised: March 12, 2018

Accepted: March 13, 2018

Published: April 10, 2018

REFERENCES

- Abu-Shaar, M., Ryoo, H.D., and Mann, R.S. (1999). Control of the nuclear localization of Extradenticle by competing nuclear import and export signals. *Genes Dev.* *13*, 935–945.
- Agoston, Z., Heine, P., Brill, M., Grebbin, B., Hau, A.-C., Kallenborn-Gerhardt, W., Schramm, J., Götz, M., and Schulte, D. (2014). *Meis2* is a Pax6 co-factor in neurogenesis and dopaminergic periglomerular fate specification in the adult olfactory bulb. *Development* *141*, 28–38.
- Beckervordersandforth, R., Tripathi, P., Ninkovic, J., Bayam, E., Lepier, A., Stempfhuber, B., Kirchhoff, F., Hirrlinger, J., Haslinger, A., Lie, D.C., et al. (2010). In vivo fate mapping and expression analysis reveals molecular hallmarks of prospectively isolated adult neural stem cells. *Cell Stem Cell* *7*, 744–758.
- Berthelsen, J., Zappavigna, V., Ferretti, E., Mavilio, F., and Blasi, F. (1998). The novel homeoprotein Prep1 modulates Pbx-Hox protein cooperativity. *EMBO J.* *17*, 1434–1445.



- Berthelsen, J., Kilstrup-Nielsen, C., Blasi, F., Mavilio, F., and Zappavigna, V. (1999). The subcellular localization of PBX1 and EXD proteins depends on nuclear import and export signals and is modulated by association with PREP1 and HTH. *Genes Dev.* *13*, 946–953.
- Cox, J., and Mann, M. (2008). MaxQuant enables high peptide identification rates, individualized p.p.b.-range mass accuracies and proteome-wide protein quantification. *Nat. Biotechnol.* *26*, 1367–1372.
- Doetsch, F., Petreanu, L., Caille, I., Garcia-Verdugo, J.M., and Alvarez-Buylla, A. (2002). EGF converts transit-amplifying neurogenic precursors in the adult brain into multipotent stem cells. *Neuron* *36*, 1021–1034.
- Hau, A.C., Grebbin, B.M., Agoston, Z., Anders-Maurer, M., Müller, T., Groß, A., Kolb, J., Langer, J.D., Döring, C., and Schulte, D. (2017). MEIS homeodomain proteins facilitate chromatin opening through PARP1/ARTD1-mediated eviction of histone H1. *J. Cell Biol.* *216*, 2715–2729.
- Hsieh, J. (2012). Orchestrating transcriptional control of adult neurogenesis. *Genes Dev.* *26*, 1010–1021.
- Imayoshi, I., Sakamoto, M., Ohtsuka, T., Takao, K., Miyakawa, T., Yamaguchi, M., Mori, K., Ikeda, T., Itohara, S., and Kageyama, R. (2008). Roles of continuous neurogenesis in the structural and functional integrity of the adult forebrain. *Nat. Neurosci.* *11*, 1153–1161.
- Kempermann, G., Kuhn, H.G., and Gage, F.H. (1997). More hippocampal neurons in adult mice living in an enriched environment. *Nature* *386*, 493–495.
- Knoepfler, P.S., Calvo, K.R., Chen, H., Antonarakis, S.E., and Kamps, M.P. (1997). Meis1 and pKnox1 bind DNA cooperatively with Pbx1 utilizing an interaction surface disrupted in oncoprotein E2a-Pbx1. *Proc. Natl. Acad. Sci. USA* *94*, 14553–14558.
- Ladam, F., and Sagerström, C.G. (2014). Hox regulation of transcription: more complex(es). *Dev. Dyn.* *243*, 4–15.
- Longobardi, E., Penkov, D., Mateos, D., De Florian, G., Torres, M., and Blasi, F. (2014). Biochemistry of the tale transcription factors PREP, MEIS, and PBX in vertebrates. *Dev. Dyn.* *243*, 59–75.
- Mamo, A., Kros, J., Kroon, E., Bijl, J., Thompson, A., Mayotte, N., Girard, S., Bisailon, R., Beslu, N., Featherstone, M., et al. (2006). Molecular dissection of Meis1 reveals 2 domains required for leukemia induction and a key role for Hoxa gene activation. *Blood* *108*, 622–629.
- Mercader, N., Leonardo, E., Azpiazu, N., Serrano, A., Morata, G., Martínez, C., and Torres, M. (1999). Conserved regulation of proximodistal limb axis development by Meis1/Hth. *Nature* *402*, 425–429.
- Ming, G.L., and Song, H. (2011). Adult neurogenesis in the mammalian brain: significant answers and significant questions. *Neuron* *70*, 687–702.
- Paul, A., Chaker, Z., and Doetsch, F. (2017). Hypothalamic regulation of regionally distinct adult neural stem cells and neurogenesis. *Science* *356*, 1383–1386.
- Sakamoto, M., Imayoshi, I., Ohtsuka, T., Yamaguchi, M., Mori, K., and Kageyama, R. (2011). Continuous neurogenesis in the adult forebrain is required for innate olfactory responses. *Proc. Natl. Acad. Sci. USA* *108*, 8479–8484.
- Schulte, D. (2014). Meis: new friends of Pax. *Neurogenesis* *1*, e976014.
- Shingo, T., Gregg, C., Enwere, E., Fujikawa, H., Hassam, R., Geary, C., Cross, J.C., and Weiss, S. (2003). Pregnancy-stimulated neurogenesis in the adult female forebrain mediated by prolactin. *Science* *299*, 117–120.
- Wang, G.G., Pasillas, M.P., and Kamps, M.P. (2006). Persistent transactivation by meis1 replaces hox function in myeloid leukemogenesis models: evidence for co-occupancy of meis1-pbx and hox-pbx complexes on promoters of leukemia-associated genes. *Mol. Cell. Biol.* *26*, 3902–3916.

Stem Cell Reports, Volume 10

Supplemental Information

**Arginine Methylation Regulates MEIS2 Nuclear Localization to Promote
Neuronal Differentiation of Adult SVZ Progenitors**

**Jasmine Kolb, Marie Anders-Maurer, Tanja Müller, Ann-Christin Hau, Britta Moyo
Grebbin, Wiebke Kallenborn-Gerhardt, Christian Behrends, and Dorothea Schulte**

Supplemental Figures

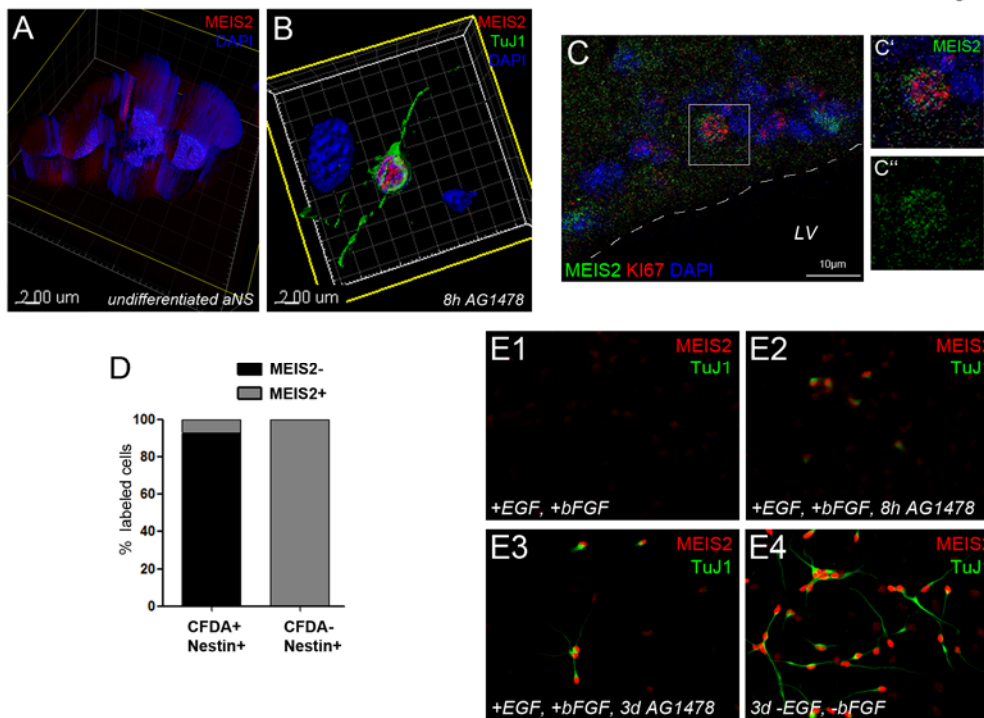


Figure S1. MEIS2 in adult SVZ-derived stem- and progenitor cells *in vivo* and *in vitro*. (A, B) 3D-reconstruction of serial confocal laser scanning micrographs of primary SVZ-derived aNS (A) or an *in vitro* differentiated TuJ1-labeled neuron obtained by plating on laminin and treatment with AG1478 (B). MEIS2-staining (red) is weak and not confined to the cell nucleus in adult neural progenitor cells, the primary component of aNS (A), but strong and nuclear in neurons, recognized by their immunoreactivity for the TuJ1-epitope (green; B). (C) Weak, uniform MEIS2-staining in cells that exhibit nuclear Ki67-immunoreactivity, presumably TAPs, in the SVZ *in vivo*. (D) Proportion of label-retaining (CFDA+) or label non-retaining (CFDA-), nestin-expressing cells that exhibit immunoreactivity for MEIS2. Putative transient amplifying cells (defined as CFDA-negative, nestin-expressing cells) exhibited uniform MEIS2-immunoreactivity in the cytoplasm and nucleus, whereas the vast majority of label-retaining, nestin-expressing cells (putative stem cells) did not stain for MEIS2. The few nestin+/CFDA+ cells that co-labeled with the MEIS2-specific antibody may either represent a minor population of label-retaining *Meis2*-expressing cells or, more likely, correspond to transient

amplifying cells that had been generated from label-retaining cells shortly before the cells were fixed and analyzed and therefore had not yet fully lost the CFDA-label. (E) Primary aNS grown as adherent cultures under different culture conditions; the images shown in panels 1-4 were taken with identical exposure times to highlight the strong increase in MEIS2 staining observed upon neuronal differentiation. (E1) MEIS2 immunoreactivity is very low in cells growing in the presence of EGF and FGF2; (E2) Addition of AG1478 elicits nuclear accumulation of MEIS2 in some cells of the culture, these cells stain positive for TuJ1; (E3) Appearance of TuJ1+ neurites in cells with nuclear MEIS2 staining upon prolonged differentiation times; (E4) typical staining for MEIS2 and TuJ1 in primary SVZ neurospheres differentiated for 3 days by withdrawal of EGF and FGF2 from the medium.

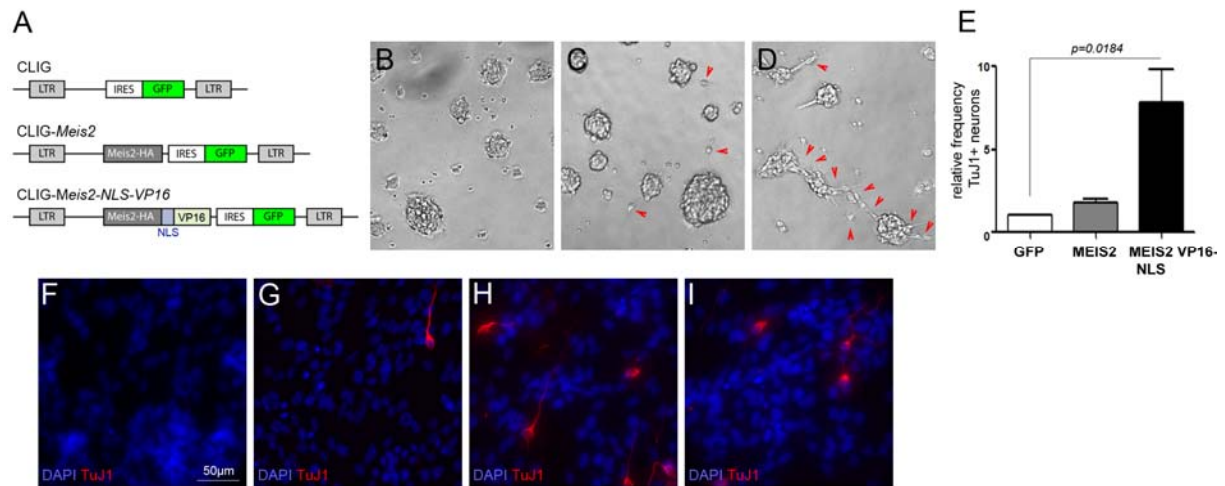


Figure S2. Retroviral misexpression of a transactivating fusion protein of *Meis2* in SVZ-derived aNS induces neuronal differentiation in EGF/FGF2 containing medium. (A) Schematic drawing of the retroviral vectors used. (B-D) Light microscopy images of aNS cultures growing as free-floating spheres in the presence of EGF and FGF2 and transduced with different viral vectors; viruses expressing only GFP (B), viral vectors carrying *Meis2* together with GFP (C), and viral vectors carrying *Meis2* C-terminally fused to a NLS and the VP16 transactivation domain (D). Red arrowheads indicate cells or groups of cells, which have attached to the cell culture flask and show the typical, bipolar morphology of differentiating neuroblasts. (E) Relative frequency of TuJ1+ neurons among cells transduced with the indicated retroviruses in aNS cultures growing in EGF/FGF2 containing medium. Transduction of *Meis2-VP16-NLS* induces substantial neuronal differentiation; n=3. Data are represented as mean \pm SEM. (F-I) Representative, high-magnification images of TuJ1-immunoreactive cells generated from free-floating aNS growing in EGF/FGF2-containing medium and transduced with GFP (F), *Meis2* (G) or *Meis2-VP16-NLS* (H, I). The scale bar in (F) also applies to (G-I).

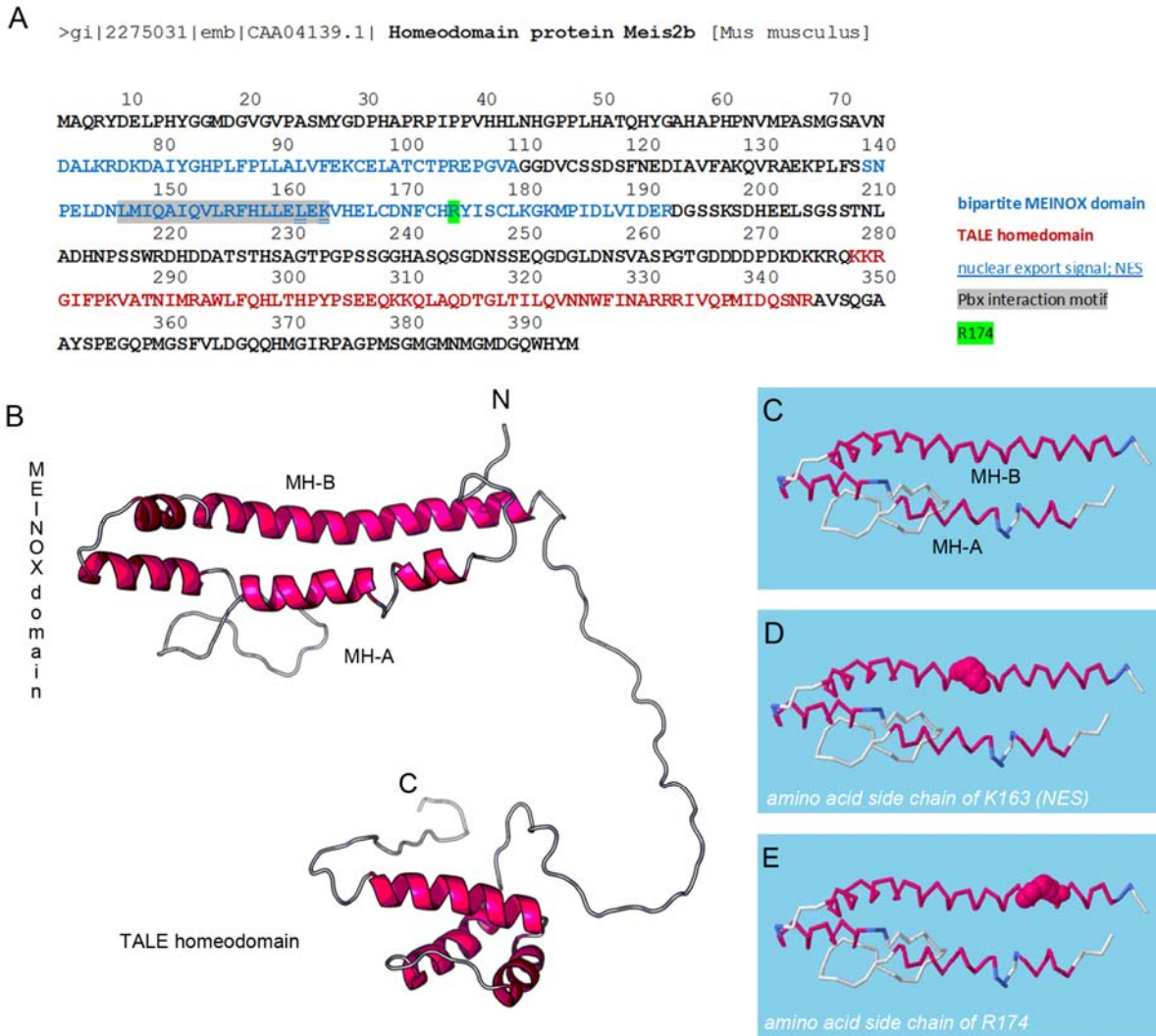


Fig. S3. Protein structure prediction of MEIS2. (A) Protein sequence of mouse MEIS2b; the bipartite MEINOX domain with the MH-A and MH-B subdomains is shown in blue, the TALE homeodomain in red. NES, the PBX-binding motif (as determined by (Knöpfler et al., 1997)) and R174 are underlined or shaded respectively. (B) Protein structure of MEIS2B as predicted by RaptorX (<http://raptorx.uchicago.edu>). (C-E) Schematic drawings of the MEINOX domain; the predicted orientation of the amino acid side chains of arginine 174 and lysine 163, an integral part of the LLELEK nuclear export motif, are shown in (E) and (D) respectively. Note that both amino acids are located within a predicted alpha helical structure with both side chains facing the same orientation.

Knoepfler, P.S., Calvo, K.R., Chen, H., Antonarakis, S.E., and Kamps, M.P. (1997). Meis1 and pKnox1 bind DNA cooperatively with Pbx1 utilizing an interaction surface disrupted in oncoprotein E2a-Pbx1. *Proc. Natl. Acad. Sci. U.S.A.* *94*, 14553-8.

Supplemental Experimental Procedures

Cultivation of primary stem-/progenitor cell cultures of the SVZ under free-floating and adherent conditions

All procedures involving animals were approved by the local animal care committee and the government of Hessen, and are in accordance with German and EU regulations. Neurospheres (aNS) were prepared from 7-10 week old C57bl6 mice and cultured in DMEM/F-12 containing 3.5 mM glucose (GIBCO), B-27 supplement (GIBCO), 20 ng/ml fibroblast growth factor-2 (FGF2, human recombinant; Peprotech) and 20 ng/ml epidermal growth factor (EGF, human recombinant; Peprotech) as described (Agoston et al., 2014). Unless noted otherwise, primary aNS, grown as free-floating spheres for no more than five days in the presence of EGF/FGF2 without attachment to laminin were used. To assess MEIS2 subcellular localization, aNS cells were split with accutase, resuspended in EGF/FGF2-containing culture medium and briefly allowed to attach to coverslips that had been coated with poly-D lysine. To induce cellular differentiation, aNS cells were split with accutase and plated on coverslips coated with ($1\mu\text{g}/\text{cm}^2$ laminin (Roche) in medium lacking EGF and FGF2 and cultivated for the times indicated. The images in Fig. S1E show adherent neurosphere cultures. For these, cells were allowed to attach to cell culture dishes coated with ($1\mu\text{g}/\text{cm}^2$ laminin (Roche), in EGF/FGF2-containing medium. For retroviral infection, neurospheres split with accutase, washed once with EGF/FGF2 containing medium, resuspended in 1.2ml EGF/FGF2 containing medium and incubated for 4 hours at 37°C in the presence of retroviral stocks at $1-3 \times 10^5$ CFU/ml. Cells were then pelleted for 2min at 4.200 rpm in an Eppendorf centrifuge at room temperature, washed again once, resuspended in 5ml EGF/FGF2-containing medium and allowed to grow under non-adherent conditions for additional 48 hours. The following pharmacological agents were used: AdOX (Sigma Aldrich, A7154) 10 μM (from a 1mM stock in distilled water); AG1478 (N-(3-Chlorophenyl)-6,7-dimethoxy-4-quinazolinamine; LC-Laboratories, T-7310) 100nM (from a 10mM stock in DMSO); SU5402 (3-[3-(2-Carboxyethyl)-4-methylpyrrol-2-methylidanyl]-2-indolinone; Santa

Cruz, sc-204308) 20 μ M (from a 10mg/ml stock in DMSO); Leptomycin B (Sigma, L2913) 50nM (from a 10 μ M stock in Methanol). Control cells were treated with equal volumes of the respective solvent.

Retroviral constructs

Full length Meis2b was amplified with the primers 5'-TACCAATTGCATGGCGCAAAGGTACGAT and 5'-TAGCTAGCCATATAGTGCCACTGCCCATC from cDNA prepared from the SVZ of adult C57Bl/6 mice and cloned MfeI and NheI into the EcoRI and NheI sites of pSLAX13-HA (generous gift of Cliff Tabin, Harvard Medical School, Addgene #14027), which generates a C-terminal fusion to a triple HA-epitope to allow immunohistochemical differentiation between endogenous MEIS2 and the retrovirally misexpressed transgene. The mMeis2b-HA insert was isolated by XbaI digest, blunted and cloned into the pCLIG retroviral vector (Hojo et al., 2000). pCLIG carries an IRES-GFP cassette for visualization of the transduced cells. For CLIG-Meis2-NLS, an oligonucleotide corresponding to the nuclear localization signal of SV40 large T-antigen (PKKKRKV) (Kalderon et al., 1984) was inserted in frame into NdeI/SacI sites of the last HA-tag of mMeis2b-HA. For CLIG-MEIS2-NES, an oligonucleotide corresponding to the sequence LPPLERLTL (Fischer et al., 1995) was inserted in frame into NdeI/SacI sites of the last HA-tag of mMeis2b-HA. In CLIG-Meis2-NLS-VP16, mMEIS2b-HA was C-terminally fused to the NLS of SV40 large T-antigen followed by an in frame fusion to the herpes simplex virion protein 16 (VP16) transactivation domain. To generate CLIG-MEIS2-R174A the arginine at position 174 of mMeis2b-HA was converted into alanine by site directed mutagenesis (Phusion Site-Directed Mutagenesis Kit, Thermo Scientific, F-541) following manufacturer's instructions.

CFDA-labeling

Primary neurospheres were dissociated with accutase (Sigma Aldrich) 24 hours prior to labeling. CFDA labeling occurred in 2.5 μ M CFDA (carboxyfluorescein diacetat succinimidyl ester; Invitrogen, C1354) in Dulbecco's PBS (Invitrogen) for 5 min. at room temperature. Cells were washed in culture medium and once more after 1 hour of incubation at 37°C. The cells were grown as free-floating aNS and passaged every three days by dissociation with accutase for a total of three passages. After the

last split, the cells were allowed to adhere to laminin coated slides, fixed in 2% paraformaldehyde in Dulbecco's PBS and stained with MEIS2- and nestin-specific antibodies.

Quantitative real-time PCR

Total RNA was isolated from murine SVZ-derived progenitor cells passage 1-2 utilizing RNeasy Mini Kit (Qiagen) including on-column DNase digestion (Qiagen, RNase-free DNase set) to eliminate remaining genomic DNA. RNA quality and quantity was assessed using a NanoDrop spectrophotometer. 1µg RNA was reversely transcribed with the First Strand cDNA Synthesis Kit (Thermo Scientific) with random hexamer primers according to the manufacturer's instructions. Complementary DNA corresponding to 5ng of total RNA was subjected to qPCR using Absolute qPCR SYBR Green Mix (Thermo Scientific) and a CFX Real-Time PCR Detection System (BioRad). Relative target gene expression was normalized to the housekeeping gene β -actin. Relative expression was calculated with the $\Delta\Delta Cq$ calculation method, normalizing first on housekeeping gene $\Delta Cq = Cq_{(TAR)} - Cq_{(REF)}$ followed by transformation to exponential expression $\Delta Cq = 2^{-\Delta Cq}$. Primer sequences were:

Meis1: 5`-TTGGAATTAGAGAAGGTACACGAA and 5`-TGGATAATTTGATGATACAAGCA;

Meis2: 5`-AGGTGATGACGACGATCCAG and 5`-GGCATTGATAAACCAGTTGTTCC;

DCX: 5'-GGAAGGGGAAAGCTATGTCTG and 5'-TTGCTAGCCAAGGACTG;

β -actin: 5'-AGCCATGTACGTAGCCATCC and 5'-CTCTCAGCTGTGGTGGTGAA.

Antibodies and immunohistochemistry

The following primary antibodies were used: α -TUBULIN, mouse monoclonal (Abcam, ab-7291), WB (Western Blot): 1:40.000, IFC (immunofluorescence): 1:2.000; HA-HRP, rat monoclonal (3F10. Roche Diagnostics, 12 013 819 001), WB: 1:10.000; anti HA; rat monoclonal (3F10. Roche Diagnostics, 12 013 819 001) IFC 1:1.000; Ki67, mouse monoclonal (clone16A8, BioLegend, 652401) IFC: 1:200; MEIS2, rabbit polyclonal (gift of Arthur Buchberg, Arthur Buchberg, Kimmel Cancer Center, Pennsylvania), WB: 1:20.000, IFC: 1:5.000; MEIS2, mouse monoclonal (Sigma Aldrich, WH0004212M1), WB: 1:2.000, IFC: 1:200; NESTIN mouse monoclonal b (Chemicon, MAB252), IFC

1:500; neuronal β III-TUBULIN (TuJ1), mouse monoclonal (Covance, MMS-435P), IFC: 1:1.000; PBX1, rabbit polyclonal (Cell Signaling Technologies, 4342) WB: 1:1.000, IFC: 1:400; PREP1 / MEIS4 clone 1.1, mouse monoclonal (Upstate, 05-766) WB: 1:10.000; PSA-NCAM, mouse monoclonal (Millipore, MAB5324), IFC 1:1.000. Secondary antibodies for immunohistochemistry were Alexa 594-, Alexa 488-, Cy2 or Cy3 conjugated (Molecular Probes, OR, Invitrogen, Karlsruhe, Germany or Dianova, Hamburg, Germany). Some sections were counterstained with 4'-6-Diamidino-2-phenylindole (DAPI) to visualize cell nuclei. For immunostaining, cells or fresh cryosections were fixed for 10 min. at room temperature in 2% paraformaldehyde in Dulbecco's PBS, washed in PBS and stained over night in the presence of 5 % ChemiBlock (Millipore) or 10 % goat serum with 0.5 % Triton X 100 and the antibodies listed above. SDS-PAGE and Western Blot were performed following standard protocols.

Analyses of MEIS2-containing protein complexes

Subcellular fractionation, immunoprecipitation and GST pull-down assays were performed as described (Agoston and Schulte, 2009; Agoston et al., 2014). For immunoprecipitation (except purification of MEIS2 for mass spectrometry, see below), 2 μ g per reaction of the following antibodies were used: HA-probe, rabbit polyclonal (Santa Cruz Biotechnology, Y-11), PBX1, rabbit polyclonal (Cell Signaling Technologies, 4342), MEIS2, goat polyclonal (Santa Cruz Biotechnology, sc-10600). Isotype specific antibodies served as control (Santa Cruz Biotechnology). Secondary antibodies were Alexa 350-, Alexa 488-, Alexa 568-, Alexa 594- or Cy5-conjugated (Molecular Probes). For Western Blot analysis, proteins were separated on SDS-PAGE, transferred onto PVDF-membranes, blocked and incubated with the above antibodies following standard methods. HRP-conjugated secondary antibodies were goat-anti rabbit HRP (Cell Signaling Technologies, 1:10.000), goat-anti mouse HRP (Sigma Aldrich, 1:10.000), Immunocruz anti-mouse (Santa Cruz Biotechnology). Antibodies were diluted in 3% BSA in Tris-buffered saline or Rotiblock (Carl Roth, Karlsruhe, Germany). Blots were developed with Luminata forte (Millipore), chemiluminescence signals were detected with a LI-COR Odyssey Fc imager.

Mass-spectrometry analysis

MEIS2 protein from aNS and OB tissue was isolated by immunoprecipitation from the olfactory bulbs of eight 10-week old C57Bl/6 mice or early secondary aNS produced from 10 age matched C57Bl/6 mice per experiment. For MEIS2 isolation from aNS, primary aNS were dissociated with accutase (Sigma Aldrich) one day prior to extract preparation and 4×10^7 cells per experiment were allowed to recover over night. Preparation of cytoplasmic and nuclear extract and immunoprecipitation of MEIS2 were carried out as described (Agoston et al., 2014) and with 31.2 μ g anti-MEIS1/2 goat (Santa Cruz Biotechnology; sc-10599-X) and 120 μ g protein A dynabeads (Invitrogen) per reaction. Preparation of protein extracts from aNS was carried out in the presence of 5 μ M MG123 (Merck, 474791). Precipitates were separated by SDS-PAGE, stained with Colloidal Coomassie and the MEIS2 protein band was excised from the gel.

Liquid chromatography-tandem mass spectrometry analyses were performed on an EasyLC nano-HPLC coupled to an Orbitrap Elite mass spectrometer (both Thermo Scientific). In gel trypsin digestion of the immunoprecipitates was performed as described previously (Shevchenko et al., 2006). Briefly, eluates were run on a SDS-PAGE, alkylated with chloroacetamide, overnight digested with trypsin (Promega), and extracted. The desalted peptide mixtures were injected onto the column in HPLC Solvent A (0.5% acetic acid) and eluted with a 5%-33% gradient HPLC solvent B (80% acetonitril in 0.5% acetic acid) running at a constant flow rate of 200 nl/min at 30°C. Full-scan MS spectra were acquired in a mass range from m/z 150 to 2,000 with a resolution of 120,000 without lock mass. The 20 most intense precursor ions were sequentially CID fragmented in each scan cycle. In all measurements, up to 500-sequenced precursor masses were excluded from further analysis for 90 s. The target values of the mass analyzers were 1 million charges (MS) and 5,000 charges (MS/MS). MS data was processed using default parameters of the MaxQuant software (1.2.2.5) (Cox and Mann, 2008). The peak lists were queried against the human UniProt database (2012_04). Full tryptic specificity was required, and up to two missed cleavages were allowed. Carbamidomethylation of cysteine was set as fixed modification. Protein N-terminal acetylation,

oxidation of methionine, and methylation of arginine and lysine were set as variable modifications. Initial precursor mass tolerance was set to 7 ppm and 0.5 Da at the fragment ion level. False discovery rates were set to 1% at peptide and protein group level. The MS/MS spectra shown in Fig. 4 represent MEIS2 isolated from cytoplasmic extracts prepared from aNS (Fig. 4A) and nuclear extracts of OB tissue (Fig. 4B). R174 was neither methylated in MEIS2 precipitated from nuclear nor cytoplasmic aNS extracts. No MEIS2 protein could be detected in cytoplasmic OB-extracts.

Peptide pull-down

Peptides comprising the sequences LMIQAIQVLRFHLLLEKVVHELCDNFCHRYISCLK and LMIQAIQVLRFHLLLEKVVHELCDNFCHR{met}YISCLK, N-terminally linked to a mini-PEG linker followed by biotin were purchased from ProteoGenix (Schiltigheim, France). Peptides were immobilized on streptavidin-coated dynabeads (Invitrogen) essentially as described in (Dormann et al., 2012) with the following modifications: 200 pmol peptide per 10 μ l beads were coupled in binding buffer (20mM sodium phosphate buffer pH 7.4, 150mM KCl, 0.5mM EDTA, 5mM MgCl₂, 10% Glycerol, complete protease inhibitor cocktail (Roche)). Beads were washed four times in blocking buffer (binding buffer supplemented with 0.1% BSA), blocked for 12 min and washed once in binding buffer supplemented with 0.01% Tween20. Recombinant PBX1 and CRM1-HA were generated from pCS2-Pbx1a (gift of L. Selleri, Weill Cornell Medical College) and pRK5-Crm1HA (gift of R. Kehlenbach University Medical School Göttingen (Roloff et al., 2013)) respectively by TNT-coupled transcription/translation following the manufacturer's instructions (Promega). 60 μ l reactions each were diluted to 600 μ l with water and increasing volumes of the respective proteins were incubated with 10 μ l peptide-coupled beads for 2 hours at 4°C. Thereby, 1 arbitrary unit (a.u.) in Figs. 3 and 4 corresponds to 10 μ l of the diluted *in vitro* translated proteins (e.g. 6 a.u. equal 60 μ l (or 10%) of the 600 μ l IVT reaction). For competitive pull-down assays, 30 μ l PBX1 were incubated with the beads for 30 min prior to addition of the indicated amounts of CRM1-HA. After the incubation period, the beads were washed four times with binding buffer supplemented with 0.01% Tween20; bound proteins were eluted in 1x LDS-

sample buffer (Novex) and heated to 95°C for 5 min. This treatment also removed the biotinylated peptides from the streptavidin matrix. Eluted proteins and peptides were separated on a 8-16% Tris-Glycine gradient gel (Novex), transferred to PVDF-membranes and detected with antibodies specific for PBX1 and the HA-epitope respectively. Blots were stripped and re-probed with streptavidin-HRP to detect the biotinylated peptides. For the graph shown in Fig. 4O, band intensities were quantified with ImageJ and normalized to the band achieved with 10µl of the diluted *in vitro* translated proteins (i.e. input of 1 a.u.).

Reporter assay

The luciferase reporter construct DCX2073 contains the genomic fragment of NT -3838 to NT -1765 upstream of the DCX start codon (corresponding to pdcx2kb of (Piens et al., 2010)) subcloned into pGL3basic (Promega) and was previously described in Agoston et al., 2014. HEK293T cells were chosen for reporter assays because of their low endogenous Meis2 expression. Cells were transfected with 140ng of the above reporter constructs together with 40fmol each of Pbx1b-pCS2+, Meis2b-pMIWIII and Pax6(-5a)-pMIWIII. A plasmid expressing Renilla luciferase under the control of the human elongation factor 1 (Hef-1) promoter was co-transfected for normalization, luciferase assays were performed in triplicates 48 hours after transfection according to (Dyer et al., 2000).

In silico analysis of protein motifs

The NES motif in MEIS2 was identified according to (Cour et al., 2004) (<http://www.cbs.dtu.dk/services/NetNES/>). NLS sequences were analyzed based on models by Kosugi and colleagues (http://nls-mapper.iab.keio.ac.jp/cgi-bin/NLS_Mapper_form.cgi; (Kosugi et al., 2008; 2009a; 2009b)). Protein secondary structure prediction was carried out using Psipred (<http://bioinf.cs.ucl.ac.uk/psipred/>) and RaptorX (<http://raptorx.uchicago.edu/>; (Källberg et al., 2012)).

Data acquisition and statistical analysis

Images were taken with a Nikon 80i, confocal images with a Nikon Eclipse TE2000-E and a 63 oil immersion lens with optical sections of maximum 1–2 μm intervals. A minimum of 300 cells per condition and experimental repeat were photographed. The number of independent experiments is given in the figure legends as 'n= *number of independent experiments*'. Standard deviation was calculated between independent experiments. Error bars represent s.e.m. Comparison between two groups was performed with unpaired student's t-test or non-parametrical Mann-Whitney U test when normal distribution of the data could not be assumed. Comparison between three or more groups was carried out by one-way ANOVA followed by Bonferoni Multiple Comparison post-hoc test (Prism 5.01, Graph Pad). Because the immunohistochemical staining intensity for MEIS2 obtained in primary aNS is significantly lower than that seen in *in vitro* differentiated neurons, neurons of the OB or in SK-N-Be(2) cells, contrast settings had to be adjusted automatically across the entire image to visualize the subcellular distribution of MEIS2 protein in aNS. The intensities of the MEIS-specific immunofluorescence shown in Fig.1B-G, 2B, C, and 4C, D, F, G, J, K therefore slightly overestimate the actual MEIS2 protein present in the cells. An unbiased account of the relative protein expression levels of MEIS2 in undifferentiated, SVZ-derived progenitor cells and differentiated neurons can be seen in Fig. S1E₁-E₄, which show aNS grown as adherent cultures on laminin (Fig. S1E₁) and at different times after cellular differentiation was induced by addition of AG1478 (Fig. S1E₂, S1E₃) or removal of EGF and FGF2 from the culture medium (Fig. S1E₄).

Supplemental references

Agoston, Z., and Schulte, D. (2009). Meis2 competes with the Groucho co-repressor Tle4 for binding to Otx2 and specifies tectal fate without induction of a secondary midbrain-hindbrain boundary organizer. *Development* *136*, 3311-22.

Agoston, Z., Heine, P., Brill, M.S., Grebbin, B.M., Hau, A., Kallenborn-Gerhardt, W., Schramm, J., Götz, M., and Schulte, D. (2014). Meis2 is a Pax6 co-factor in neurogenesis and dopaminergic periglomerular fate specification in the adult olfactory bulb. *Development* *141*, 28-38.

Cour, T.L., Kiemer, L., Mølgaard, A., Gupta, R., Skriver, K., and Brunak, S. (2004). Analysis and prediction of leucine-rich nuclear export signals. *Protein Engineering, Design & Selection : PEDS* *17*, 527-36.

Cox, J., and Mann, M. (2008). MaxQuant enables high peptide identification rates, individualized p.p.b.-range mass accuracies and proteome-wide protein quantification. *Nature Biotechnology* *26*, 1367-72.

Dormann, D., Madl, T., Valori, C.F., Bentmann, E., Tahirovic, S., Abou-Ajram, C., Kremmer, E., Ansorge, O., Mackenzie, I.R.A., Neumann, M., et al. (2012). Arginine methylation next to the PY-NLS modulates Transportin binding and nuclear import of FUS. *The EMBO Journal* *31*, 4258-75.

Dyer, B.W., Ferrer, F.A., Klinedinst, D.K., and Rodriguez, R. (2000). A noncommercial dual luciferase enzyme assay system for reporter gene analysis. *Analytical Biochemistry* *282*, 158-61.

Fischer, U., Huber, J., Boelens, W.C., Mattaj, I.W., and Lührmann, R. (1995). The HIV-1 Rev activation domain is a nuclear export signal that accesses an export pathway used by specific cellular RNAs. *Cell* *82*, 475-83.

Hojo, M., Ohtsuka, T., Hashimoto, N., Gradwohl, G., Guillemot, F., and Kageyama, R. (2000). Glial cell fate specification modulated by the bHLH gene Hes5 in mouse retina. *Development* *127*, 2515-22.

Kalderon, D., Roberts, B.L., Richardson, W.D., and Smith, A.E. (1984). A short amino acid sequence able to specify nuclear location. *Cell* *39*, 499-509.

Kosugi, S., Hasebe, M., Entani, T., Takayama, S., Tomita, M., and Yanagawa, H. (2008). Design of peptide inhibitors for the importin alpha/beta nuclear import pathway by activity-based profiling. *Chem. Biology* *15*, 940-9.

Kosugi, S., Hasebe, M., Matsumura, N., Takashima, H., Miyamoto-Sato, E., Tomita, M., and Yanagawa, H. (2009a). Six classes of nuclear localization signals specific to different binding grooves of importin alpha. *J. Biol. Chem.* *284*, 478-85.

Kosugi, S., Hasebe, M., Tomita, M., and Yanagawa, H. (2009b). Systematic identification of cell cycle-dependent yeast nucleocytoplasmic shuttling proteins by prediction of composite motifs. *Proc. Natl. Acad. Sci. U.S.A.* *106*, 10171-6.

Källberg, M., Wang, H., Wang, S., Peng, J., Wang, Z., Lu, H., and Xu, J. (2012). Template-based protein structure modeling using the RaptorX web server. *Nature Protocols* *7*, 1511-22.

Piens, M., Muller, M., Bodson, M., Baudouin, G., and Plumier, J. (2010). A short upstream promoter region mediates transcriptional regulation of the mouse doublecortin gene in differentiating neurons. *BMC Neuroscience* *11*, 64.

Roloff, S., Spillner, C., and Kehlenbach, R.H. (2013). Several phenylalanine-glycine motives in the nucleoporin Nup214 are essential for binding of the nuclear export receptor CRM1. *J. Biol. Chem.* *288*, 3952-63.

Shevchenko, A., Tomas, H., Havlis, J., Olsen, J.V., and Mann, M. (2006). In-gel digestion for mass spectrometric characterization of proteins and proteomes. *Nature Protocols* *1*, 2856-60.